Intrinsic thermoacoustic modes in an annular combustion chamber

Philip E. Buschmann[a,*], Georg A. Mensah[b], Jonas P. Moeck[a]

[a] *Department of Energy and Process Engineering*
Norwegian University of Science and Technology
Trondheim, Norway
[b] *CAPS Laboratory*
Department of Mechanical and Process Engineering
ETH Zurich
Zurich, Switzerland

Abstract

Thermoacoustic instabilities originate from the interaction of unsteady heat release rate associated with flames and the acoustic modes of a combustor. A feedback loop not involving the natural acoustic modes has been observed in single-flame configurations with anechoic terminations: an acoustic wave emitted by the flame travels upstream, and the associated velocity fluctuation again excites the flame. This feedback cycle gives rise to thermoacoustic modes intrinsic to the flame (ITA modes). An analytical model for an annular thermoacoustic system is formulated, and the existence of intrinsic modes of various azimuthal orders is demonstrated. The spectrum of an annular combustor is computed with a three-dimensional thermoacoustic Helmholtz solver. The configuration resembles those commonly found in gas turbines. In addition to the observations in previous studies, numerous intrinsic modes are found, with frequencies close to the lowest acoustic modes. All of the intrinsic modes can be grouped into clusters, at frequencies corresponding to multiples of the inverse flame response time delay. It is demonstrated that the newly observed intrinsic modes belong to the same mechanism that has recently been studied in single-sector/flame configurations. An analysis of the evanescent character of cut-off azimuthal modes explains the pattern in the spectrum. The underlying physical mechanism is generically present in any annular combustion chamber and a possible source of instability.

Keywords: thermoacoustic instabilities, combustion dynamics, annular combustor, intrinsic thermoacoustic modes

1. Introduction

Modern combustion systems with high power densities, such as rocket engines and gas turbines, are prone to an unstable coupling between acoustic waves and the fluctuating heat release rate generated by one or multiple flames. In particular, annular combustion chambers enable high power densities in a compact fashion [1]. This combination is especially advantageous in aerospace applications where weight reduction is essential, but it is also favored in many stationary applications since the small surfaces in the combustor require minimal cooling. A positive feedback loop between the fluctuating heat release rate and the acoustic waves causes a growth in amplitude of the pressure oscillation: a thermoacoustic instability (TAI) manifests in the system. Combustion instabilities resulting from thermoacoustic interaction cause significant mechanical wear and potentially result in catastrophic failure of the combustion system [2]. Avoiding this undesirable unsteady phenomenon is, thus, crucial for gas turbine operation.

Numerical modeling tools are essential in identifying designs that are susceptible to TAIs at an early stage. Modeling of TAIs can be conducted based on large-eddy simulations (LES) [3, 4], linearized Navier–Stokes/Euler equations [5, 6],

*Corresponding author
Email address: philip.e.buschmann@ntnu.no (Philip E. Buschmann)

thermoacoustic Helmholtz models [7] or low-order acoustic networks [8, 9, 10]. Solving the three-dimensional thermoacoustic Helmholtz equation has been successful in predicting TAIs in realistic configurations [11, 12, 13], with significantly smaller numerical cost than LES, but having fewer modeling assumptions than network-based approaches. Linear stability analysis of the thermoacoustic system solves for the thermoacoustic modes, the complex eigenfrequencies ω with associated mode shape (or eigenfunction) $\hat{p}$, and determines whether these are amplified or attenuated in time. In the present work, we refer to a pair $(\omega, \hat{p})$ as a *mode*. The design of the system is geared towards achieving thermoacoustic stability by ensuring that all modes are damped. Evidently, this requires computing all $\omega \in \mathbb{C}$ in a relevant frequency range.

1.1. Thermoacoustic feedback mechanisms

Fluctuations in the heat release rate of the flame in a combustor emits pressure waves. These are reflected at the boundaries and travel back to cause a new perturbation of the flame [14]. This feedback loop is usually related to the natural acoustic resonance frequencies of the combustion system. From a modeling perspective, the Helmholtz equation describing the purely acoustic system is extended with a feedback term accounting for the active flame effect. This feedback term is commonly expressed in terms of the flame transfer function and, thus, depends nonlinearly on the eigenfrequency, but linearly on the mode shape. The flame feedback causes a shift in frequency and amplification or attenuation of the resonant modes. If the flame feedback is considered as a perturbation of the purely acoustic system, the thermoacoustic modes of acoustic origin are expected to be in the vicinity of the purely acoustic resonance frequencies.

In recent experiments, Hoejimakers [15] introduced anechoic terminations to a single-flame setup and observed the manifestation of a TAI. This experiment is surprising in the sense that an increased damping at the boundaries, due to the anechoic terminations, renders the system unstable – a situation that appears paradoxical.

As Hoejimakers [15] interrupted any acoustic feedback via the boundaries, an independent mechanism must be responsible for the onset of the TAI. Analysis of network models by Hoeijmakers et al. [16], Bomberg et al. [17], and Emmert et al. [18] showed that another feedback loop exists that does not require acoustic wave reflection at the boundaries. Instead, this so-called intrinsic feedback loop rests on the velocity fluctuation associated with the flame-emitted acoustic wave traveling upstream. Thus, the mechanism does not require acoustic reflection at the boundaries, as demonstrated by [19] based on an explicit solution and is solely a property of the flame response to acoustic perturbations. Consequently, the thermoacoustic modes associated with this mechanism are termed *intrinsic* (to the flame). Courtine et al. [20] gave a physical explanation for the intrinsic thermoacoustic mechanism based on a DNS study. Courtine et al.'s study in time-domain clearly shows how the intrinsic feedback loop is confined locally to the domain of the burner mouth.

Previous work [15, 16, 18, 19] showed that in a one-dimensional Rijke tube with anechoic terminations, thermoacoustic modes, which must be intrinsic for this kind of system, have the analytical solution[1]

$$\omega = \frac{\pi\,(2j+1)}{\tau} - \frac{\mathrm{i}}{\tau}\ln\left(\frac{\bar{n}}{1+\xi}\right),\ j \in \mathbb{N}^+\,, \qquad (1)$$

with $\xi = \frac{\rho_{\mathrm{cold}} c_{\mathrm{cold}}}{\rho_{\mathrm{hot}} c_{\mathrm{hot}}}$. τ is the time delay associated with the flame response to acoustic perturbations; $\bar{n}$ is the interaction index describing the gain of the response; ρ and c are mean density and mean speed of sound, respectively. The analytical solution exhibits two properties. First, high attenuation for a weakly interacting flame:

$$\mathrm{Im}\,\omega \to \infty, \quad \text{as } n \to 0, \qquad (2)$$

and, second, an equidistant frequency spacing Δf on the real line between adjacent modes (of orders $j+1$ and j), proportional to the inverse of the flame time delay:

$$\Delta f = \mathrm{Re}\left(\omega^{j+1} - \omega^{j}\right)/2\pi = 1/\tau\,. \qquad (3)$$

Recently, Mukherjee et al. [19] revisited McManus et al.'s model of the Rijke tube with reflective boundary conditions [21]. In the limit of a vanishing interaction index ($n \to 0$) Mukherjee et al. showed that strongly damped intrinsic modes have solution Eq. (1), in spite of the fact that the model does not feature anechoic terminations.

[1] We use a Fourier transform such that a time derivative $\partial_t p'$ is mapped to $+\mathrm{i}\omega\hat{p}$ in frequency domain, see Section 2.

It will be demonstrated in Section 3 and Section 5 that intrinsic modes of azimuthal type exist in annular combustion chambers with reflective boundary conditions. These modes interact with their respective cut-off frequencies. Strongly cut-off modes show an equidistant frequency spacing on the real line (Eq. (3)) even for non-vanishing n. This is a peculiarity of annular combustors, since in the single-flame setup with reflective boundary conditions Eq. (1) only holds for intrinsic modes if $n \to 0$, as shown by Mukherjee et al. [19]. Moreover, the acoustic resonance frequencies serve as no indicator for the intrinsic modes and cut-on intrinsic modes are observed in close proximity to modes of acoustic origin.

Orchini et al. [22] and Buschmann et al. [23] report intrinsic modes in annular chambers but do not explain their occurrence. To the best of the authors' knowledge, the connection of the intrinsic mechanism with azimuthal cut-off frequencies has not yet been investigated in annular combustion chambers.

Recent studies focused on the intrinsic mechanism in single-flame configurations, where it was established that intrinsic modes can be the cause of TAIs and need to be taken into account by numerical tools [24, 25, 26]. Our findings imply an equal importance for the computation of ITA modes in annular combustors.

1.2. Numerical solution of nonlinear eigenvalue problem using contour integration

Previous studies in similar settings of annular combustors [11, 27, 28, 29, 30, 31] exclusively identified modes as belonging to the acoustic feedback mechanism. It is possible, though, that intrinsic modes were computed but not identified as such. In a recent review article [13] on thermoacoustic instabilities in annular combustion chambers, intrinsic modes were not mentioned as potential sources of instabilities; however, the general relevance of intrinsic modes to annular chambers is pointed out in the review article [1].

The eigenfrequencies ω are obtained as solutions to a nonlinear eigenvalue problem (NLEVP). In general, NLEVPs cannot be cast into a form that permits an explicit solution. In thermoacoustics, these are usually solved by employing a locally convergent fixed-point strategy, initially proposed by [7] for Helmholtz solvers. This approach requires adequate initial values, such as acoustic resonance frequencies for the modes associated with the conventional feedback mechanism; however, suitable initial guesses for intrinsic modes are more difficult to provide. In the present work, a numerical solution strategy for the NLEVP was chosen that is fundamentally different from the commonly employed iterative techniques. This alternative method is based on contour integration and was suggested by Beyn [32]. It is a global strategy and determines *all* eigenfrequencies in a specified domain in the complex plane – inside a defined contour. In related work [23], the fixed-point method [7] and Beyn's method based on contour integration [32] are compared in detail with respect to their application to NLEVPs arising in thermoacoustics. A combination of Beyn's global solution algorithm and subsequent iterative local refinements[2] is used to solve all NLEVPs considered in this article. We emphasize that this strategy was essential in finding the intrinsic modes that are the main topic of this report. Incidentally, it was the interest in Beyn's global algorithm for the solution of NLEVPs that led the present authors to the discovery of the patterns of intrinsic modes discussed in the remainder of this article.

1.3. Outline of this work

The thermoacoustic Helmholtz equation, which is the basis for an analytical study and the FEM formulation, is introduced in Section 2. In Section 3 an analytical model of an annular cavity with a flame is formulated. This elementary model exhibits intrinsic modes of various azimuthal mode orders, which form a distinct pattern. A model of the MICCA combustor is formulated in Section 4. A qualitatively similar pattern of intrinsic modes is observed in the numerical study of the MICCA combustor, Sec. 5. It is explained how the intrinsic modes in the MICCA combustor originate from the intrinsic mechanism observed in axial systems. In Section 6, implications of intrinsic modes for stability analysis in annular combustion chambers are discussed.

2. Thermoacoustic model

The transport equations for mass, momentum and entropy can be linearized and then recombined

[2] For network models, this iterative local refinement is based on numerical solutions of the characteristic equation; for the FEM models, traditional fixed-point iteration is used for this purpose.

into a wave equation for the pressure fluctuation p', see [7]. Transforming the wave equation for the pressure fluctuations into frequency domain (with the convention $\partial_t p' \mapsto +\mathrm{i}\omega\hat{p}$ for the Fourier transform) yields the thermoacoustic Helmholtz equation [7]:

$$\nabla \cdot \left(c^2 \nabla \hat{p}\right) + \omega^2 \hat{p} = -\mathrm{i}\omega\left(\gamma - 1\right)\hat{q}\,, \tag{4}$$

where c is the field of the speed of sound and γ the ratio of specific heats (which is assumed to be constant). The Fourier transforms of the pressure and the heat release rate fluctuations are denoted by $\hat{p}$ and $\hat{q}$, respectively. Stability of the thermoacoustic system is determined by the eigenfrequencies $\omega \in \mathbb{C}$, where the real part of ω corresponds to the angular oscillation frequency and the negative imaginary part to the growth rate of the mode. A mode is, hence, linearly stable if $\mathrm{Im}\left(\omega\right) > 0$, and the perturbation associated with this mode experiences exponential decay. Overall thermoacoustic stability requires all modes to be damped. Since modes corresponding to higher oscillation frequencies typically experience increasingly stronger damping due to visco-thermal effects, practical stability analysis is usually restricted to modes below a threshold. A reasonable choice for a threshold is highly problem-specific and the selection of which remains at the engineer's discretion.

The equation is closed by relating $\hat{q}$ linearly to a velocity fluctuation $\hat{\mathbf{u}}$ at an upstream reference position $\mathbf{x}_{\mathrm{ref}}$ via a flame transfer function (FTF) $\mathcal{F}\left(\omega\right)$:

$$\hat{q} = \frac{\bar{Q}}{u_{\mathrm{b}} V_{\mathrm{f}}} \mathcal{F}\left(\omega\right) \hat{\mathbf{u}}_{\mathrm{ref}} \cdot \mathbf{n}_{\mathrm{ref}}\,. \tag{5}$$

Here, $\bar{Q}$ denotes the global average heat release rate and u_{b} the bulk flow velocity. In Section 3 the fraction $\bar{Q}/u_{\mathrm{b}}$ is expressed by an analytic expression in terms of a volumetric flow rate and flame-induced temperature jump, while in Section 4 values from a measurement of Laera et al. [30] are employed. In the discrete model a domain of volume V_{F} is specified which represents the flame and where the FTF acts as a volume source. The linearized impulse balance permits to express $\hat{\mathbf{u}}$ in terms of $\hat{p}$:

$$-\mathrm{i}\omega\hat{\mathbf{u}} = \frac{1}{\rho_0}\nabla\hat{p}\,, \tag{6}$$

and, thus, Eq. (4) can be expressed in $\hat{p}$ alone, if $\mathcal{F}\left(\omega\right)$ is known (e.g. from measurements, large-eddy simulations or an analytical expression).

In the present study, the n–τ model, initially proposed by [33], is employed:

$$\mathcal{F}\left(\omega\right) = n e^{-\mathrm{i}\omega\tau}\,, \tag{7}$$

where the interaction index n and time delay τ have to be specified. With suitable acoustic boundary conditions, Eqs. (4)–(7) form a closed problem that can be solved numerically; this is the subject of Sec. 4.

3. Theoretical analysis of an elementary model problem

In this section, we show that intrinsic modes of different azimuthal mode orders exist in an analytical model of an annular combustion chamber and, strikingly, exhibit a pattern which is encountered in the 3D model of Section 5. This elementary model shows that intrinsic modes generally exist in annular combustion chambers.

A model for an annulus is formulated with a pressure node at the outlet and a pressure anti-node at the inlet, see Fig. 1. Network models for annular combustion chambers were studied by [8, 34, 35]; however, the present model is considerably simpler. An active flame that is distributed homogeneously around the circumference is placed at some axial position. For an azimuthal wavenumber $m = 0$, by setting $x_{\mathrm{ref}} = L/2$ and by neglecting the effect of heat-release on mean flow quantities, this model reduces to the well-known one-dimensional thermoacoustic resonator, the Rijke tube studied in [21, 19].

3.1. Analytical model for a thin annulus with circumferential flame zone

Consider an annulus of radius R and length L with a centrally positioned flame zone over the entire circumference that separates the annulus into a cold and a hot zone, see Fig. 1. The ideal gas law for the speed of sound $c = \sqrt{\gamma \bar{R} T}$ with $\gamma = 1.4$ and $\bar{R} = 288.68\,\mathrm{J\,kg^{-1}\,K^{-1}}$ is used in the hot and cold zones. The radial dimension is neglected, and the flame response is modelled by the n–τ model with the location of the reference position x_{ref} in the cold zone left arbitrary.

In both zones, the problem is governed by the purely acoustic Helmholtz equation:

$$\nabla^2\hat{p} + \left(\frac{\omega}{c}\right)^2 \hat{p} = 0\,, \tag{8}$$

which motivates a separation ansatz in each zone:

$$\hat{p}_1(x,\theta) = X_1(x)\,\Theta(\theta)\ ,\ x \le L/2 \tag{9}$$
$$\hat{p}_2(x,\theta) = X_2(x)\,\Theta(\theta)\ ,\ L/2 < x \le L\,. \tag{10}$$

The azimuthal coordinate spans the right-open interval $\theta \in [0, 2\pi R)$. It is assumed that the flame induces a jump in the axial component alone and, thus, the azimuthal function $\Theta(\theta)$ is identical in $\hat{p}_1$ and $\hat{p}_2$. The matching conditions at the flame location x_F are the jump (denoted by square brackets) in acoustic velocity:

$$\left[c^2 \frac{\mathrm{d}\hat{p}}{\mathrm{d}x}\right]\Bigg|_{L/2-}^{L/2+} = Q(\omega)\ , \tag{11}$$

with the response given by the n–τ model:

$$Q(\omega) = \underbrace{\frac{\gamma p_0}{\rho_0}\left(\frac{T_2}{T_1}-1\right)}_{\hat{Q}} n e^{-\mathrm{i}\omega\tau}\ \frac{\mathrm{d}\hat{p}}{\mathrm{d}x}\bigg|_{x_\mathrm{ref}}\ , \tag{12}$$

and continuity in $\hat{p}$:

$$\hat{p}_1|_{\frac{L}{2}} = \hat{p}_2|_{\frac{L}{2}}\,. \tag{13}$$

Note that the interaction index here is defined differently compared to McManus et al. [21]:

$$\bar{n} = \left(\frac{T_2}{T_1}-1\right) n\,, \tag{14}$$

where $\bar{n}$ corresponds to the interaction index "n" in McManus et al. [21], which has also been noted by [19]. The formulation in Eq. (12) is consistent with the definition in Eq. (7), which is employed in the FEM model later on.

Inserting Eq. (9) and Eq. (10) into Eq. (8) allows a separation of variables. The axial wavenumbers k_j and the azimuthal wavenumber k_θ are introduced to formulate the solvability condition as:

$$\left(\frac{\omega}{c_j}\right)^2 = k_j^2 + k_\theta^2\ ,\ j = 1,2\,. \tag{15}$$

The ansatz Eq. (9) and Eq. (10) for every half $j = 1, 2$ takes the form:

$$\hat{p}_j = \left(A_j e^{\mathrm{i}k_j x} + B_j e^{-\mathrm{i}k_j x}\right)\left(E e^{\mathrm{i}k_\theta \theta} + F e^{-\mathrm{i}k_\theta \theta}\right)\,. \tag{16}$$

The constants A_1, B_1, A_2, B_2 and an expression for the azimuthal wavenumber k_θ are determined by evaluating the boundary- and matching conditions. The constants E and F in the ansatz for the azimuthal component cannot be determined for eigenfrequencies of azimuthal type due to their degeneracy. The solution has to be $2\pi R$ periodic, hence:

$$k_\theta = \frac{m}{R}\ ,\ m \in \mathbb{Z}\,, \tag{17}$$

where m is the azimuthal wavenumber, which has to be specified. Equation (15) needs to be re-arranged to obtain expressions for k_j as functions of ω and the parameter m. One of the two branches of the square root needs to be selected. The negative choice

$$k_j = -\mathrm{i}\ \sqrt[\mathrm{PV}]{\left(\frac{m}{R}\right)^2 - \left(\frac{\omega}{c_j}\right)^2}\ ,\ j = 1,2\,, \tag{18}$$

guarantees that evanescent waves have $\mathrm{Im}(k_j) \le 0$ and decay exponentially, which is the physical choice. The principle value (PV) of the complex square root is employed, since the argument is complex-valued and would yield two solutions. The present choice yields the solution with positive real part, i.e. in the right half plane. For further details see [36, p. 47].

With the chosen boundary conditions and the matching conditions, the homogeneous linear system of equations is defined through the matrix

$$\underbrace{\begin{pmatrix} 0 & e^{-\mathrm{i}k_2 L} & e^{\mathrm{i}k_2 L} \\ e^{-\mathrm{i}k_1\frac{L}{2}} + e^{\mathrm{i}k_1\frac{L}{2}} & -e^{-\mathrm{i}k_2\frac{L}{2}} & -e^{\mathrm{i}k_2\frac{L}{2}} \\ L_{31}(\omega,m) & -c_2^2(\mathrm{i}k_2)\,e^{-\mathrm{i}k_2\frac{L}{2}} & c_2^2(\mathrm{i}k_2)\,e^{\mathrm{i}k_2\frac{L}{2}} \end{pmatrix}}_{\mathbf{L}(\omega,m)}\,. \tag{19}$$

The element

$$L_{31}(\omega,m) = -c_1^2\left[(-\mathrm{i}k_1)\,e^{-\mathrm{i}k_1\frac{L}{2}} + (\mathrm{i}k_1)\,e^{\mathrm{i}k_1\frac{L}{2}}\right] - \hat{Q} n e^{-\mathrm{i}\omega\tau}\left[(-\mathrm{i}k_1)\,e^{-\mathrm{i}k_1 x_\mathrm{ref}} + (\mathrm{i}k_1)\,e^{\mathrm{i}k_1 x_\mathrm{ref}}\right] \tag{20}$$

contains the active flame effect. The linear system of equations for the coefficients B_1, A_2, and B_2 thus reads

$$\mathbf{L}(\omega,m)\begin{pmatrix} B_1 \\ B_2 \\ A_2 \end{pmatrix} = 0\,. \tag{21}$$

with $A_1 = B_1$ due to the pressure anti-node at the inlet. It is interesting to note that the matrix in Eq. (21) is identical to the 1D case [19]. The

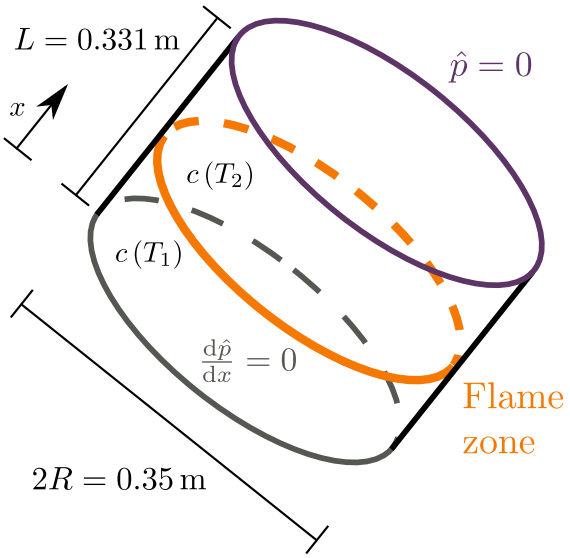

Figure 1: Schematic depiction of the annulur model. A flame zone at $x_\mathrm{F} = L/2$ spans the entire circumference and splits the domain into a cold and a hot zone: with c_1 and c_2. The reference position for the n–τ model is assumed to lay in the cold zone $x_\mathrm{ref} < x_\mathrm{F}$.

only difference is the relation between the eigenfrequency ω and the axial wavenumbers k_1 and k_2, which now involves the azimuthal wavenumber m. The 1D formulation is recovered for $m = 0$.

For fixed m, Eq. (21) exhibits non-trivial solutions only for certain values of ω, the eigenvalues, which are computed numerically in the next section.

3.2. Numerical solution of the analytical model

Eigenvalues ω of the annular model are computed by solving the dispersion relation $\det \mathbf{L}\,(\omega, m) = 0$. The physical parameters are chosen similar to the numerical study of the MICCA combustor in Sec. 4, viz. $\tau = 1.54\,\mathrm{ms}$, $T_1 = 300\,\mathrm{K}$, $T_2 = 1200\,\mathrm{K}$; see Figure 1 for the geometrical dimensions. The analytic model is not meant to represent the MICCA quantitatively.

Figure 2 shows eigenvalues of Eq. (21) for different azimuthal mode orders m in the complex plane. The mode order m can be selected arbitrarily high, but for the sake of presentation only modes up to azimuthal order $m = 10$ are shown. The interaction index is set to $n = 0.05$ ($\bar{n} = 3n$), to remain close to the limit of a weakly interacting flame. Only the part of the complex plane with high damping rates is depicted to focus on strongly damped modes. Later on it is demonstrated that these modes are of intrinsic origin and will, hence, be termed *intrinsic* even though non-anechoic boundary conditions are employed throughout this work. Any mode of a model with an active flame ($n > 0$) is generally referred to as *thermoacoustic*. This work classifies thermoacoustic modes by their behavior as $n \to 0$ into either *acoustic* ($\mathrm{Im}\,(\omega) \to 0$) or *intrinsic* ($\mathrm{Im}\,(\omega) \to +\infty$). This definition will be further explained in the next section. A precise definition of the terms *intrinsic*, *acoustic* and *thermoacoustic modes*, and the degree to which these overlap is outside the scope of this work (but see [37] and [22] for a more detailed discussion of these terms). Eigenvalues of acoustic origin are located close to the real axis due to the small interaction index.

A clear pattern is visible: modes of increasing azimuthal order line-up at certain real frequencies, forming *clusters*. These clusters are separated by approximately $\Delta f = 1/\tau$, consistent with Eq. (3). The exact value between clusters 1 and 2 (2 and 3) is $\tau_{12} = 1.510\,\mathrm{ms}$ ($\tau_{23} = 1.508\,\mathrm{ms}$), measured between modes of highest azimuthal order shown. The first cluster is at 329.70 Hz, which is close to the value of the first intrinsic mode $1/2\tau = 324.68\,\mathrm{Hz}$ according to Eq. (1). In addition, the lower the azimuthal mode order, the further offset a mode is from the rests of its respective cluster.

Figure 3 shows a peculiarity between models with different geometries: modes of lower order differ between configurations, but modes of higher order are (nearly) identical. Thus, for an intrinsic mode the mode order plays a role in the independence on the acoustic properties of the system. The discussion of the peculiarities of the eigenvalue pattern observed here are postponed until Section 5, where they are observed in the 3D MICCA combustor.

4. Numerical calculation of intrinsic modes in the MICCA annular combustor

The MICCA configuration, an annular model combustor at Laboratoire EM2C (CentraleSupélec) consists of 16 burners. It is now analyzed numerically for the presence of intrinsic modes.

4.1. Model of the MICCA combustor

The geometry and experimental data of Laera et al. [30] are used for the numerical model. Following Laera et al. [29], two geometric changes are made to the discrete model as compared to the actual experiment: an end-correction is added to the

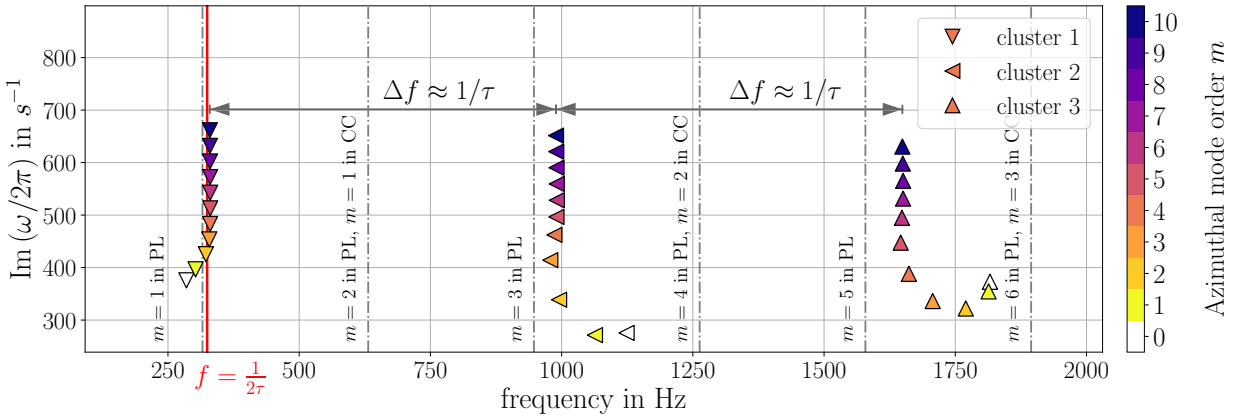

Figure 2: Intrinsic modes in the stable half-plane for $x_{\mathrm{ref}} = L/2 - 0.05\,\mathrm{m}$ and $n = 0.05$ ($\bar{n} = 3n$). The intrinsic modes of different azimuthal mode orders fan out. For every azimuthal mode number, there exist also thermoacoustic modes of acoustic origin in proximity of the real axis (not depicted here). The clusters are separated by a distance of $\Delta f \approx 1/\tau$, when the modes of highest azimuthal mode order are compared. Cluster 1 is 5 Hz off from the value $f = 1/2\tau$ of Eq. (1) for $j = 0$. Cut-off frequencies in plenum (PL) and combustion chamber (CC) are computed according to the analytic expression in [14, p. 138] and drawn as vertical gray dash-dotted lines.

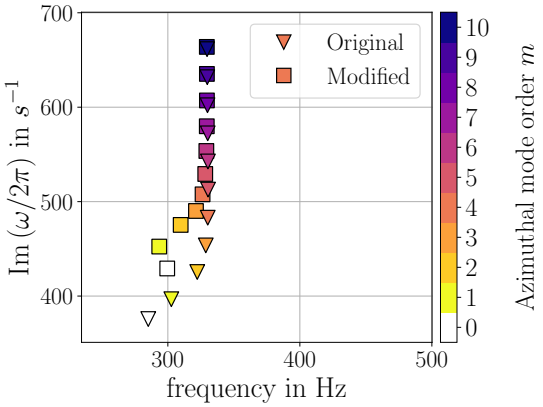

Figure 3: Eigenvalues of cluster 1 depicted in Fig. 2 (triangles) and of a longer model (squares) of twice the length with the flame zone at 1/8 of the total length (instead of half). All other parameters identical. The location of the flame zone and the length of the acoustic resonator have no effect on intrinsic modes of higher azimuthal mode orders.

combustor outlet, and the burner is modeled in a simplified manner, as a stack of two cylinders. Figure 4 shows the geometry and indicates the speeds of sound, which are set as constant in their respective cavities. Table 1 lists cut-off frequencies for the azimuthal modes of first, second and third order in the combustion chamber.

A pressure node $\hat{p} = 0$ is prescribed at the outlet, all other boundaries are set as rigid walls. The active flame parameters n and τ are taken from the experimental flame-describing function of [28]. From data for the lowest forcing amplitude ($u'/u_0 = 0.1$), the average gain is approximately $n = 0.9$. Linear regression of the phase gives $\tau = 1.54\,\mathrm{ms}$. The reference points for the n–τ model are positioned just at the inlet to the lower cylinder in the central axis of each respective burner. The flames are modeled as a flat zone spanning the floor of their individual segment with height $l_{\mathrm{F}} = 4\,\mathrm{mm}$. An average heat release rate of $\bar{Q} = 1.44\,\mathrm{kW}$ per flame and mean bulk flow velocity $u_{\mathrm{b}} = 0.49\,\mathrm{m/s}$ are set according to [29].

To ensure that the discrete model exhibits the discrete rotational symmetry of the actual combustor, the mesh of a half cell of a single combustor is first mirrored and then copied around the circumference. The mesh of the full discrete model has 38.7 k degrees of freedom.

4.2. Nonlinear eigenvalue problem

The terms in Eq. (4), closed with Eq. (7) are discretized using linear finite elements in the solver PyHoltz [38], to yield a (sparse) matrix-valued equation:

$$\mathbf{K}\mathbf{p} + \omega\mathbf{C}\mathbf{p} + \omega^2\mathbf{M}\mathbf{p} + ne^{-i\omega\tau}\mathbf{Q}\mathbf{p} = 0\,, \qquad (22)$$
$$\mathbf{K}, \mathbf{C}, \mathbf{M}, \mathbf{Q} \in \mathbb{C}^{d\times d}\,, \mathbf{p} \in \mathbb{C}^{d\times 1}\,.$$

Matrices $\mathbf{K}$ and $\mathbf{M}$ are the stiffness- and mass matrices, respectively, while $\mathbf{C}$ is related to the boundary impedance Z (here $Z = 0$ for the pressure node

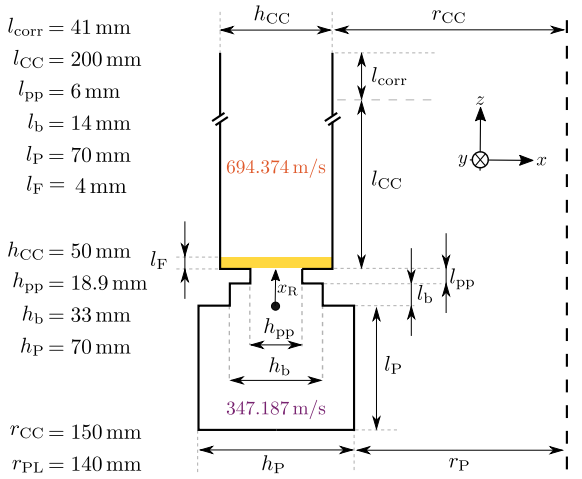

Figure 4: Cut view of a single burner in the MICCA combustor, including all geometric dimensions. The dashed line is the symmetry axis. All boundaries are set as rigid walls, except for the outlet where a pressure node is prescribed. The subscripts refer to: combustion chamber (CC), end correction (corr), flame (F), perforated plate (pp) burner (b) and plenum (PL). Temperatures are set as constant in combustion chamber and plenum.

at the outlet; rigid walls enter the FEM formulation as natural boundary conditions) and $\mathbf{Q}$ is associated with the acoustically active flame. The complex matrices have dimension d, the number of nodes in the mesh. Equation (22) contains the parameters, boundary conditions and flame response, which were listed in the previous section for the MICCA combustor.

The purely acoustic modes (or passive modes) are computed as solutions to Eq. (22) when $n = 0$ but there is still an increase in the mean temperature across the location of the flame. For the MICCA combustor, these modes are listed in Tab. 1. Solutions with $n > 0$ are referred to as active modes.

Equation (22) constitutes a nonlinear eigenvalue problem (NLEVP), which is commonly written as:

$$\mathbf{L}(\omega)\,\mathbf{p} = 0\,. \tag{23}$$

The solutions are the eigenpairs $(\omega, \mathbf{p})$; at the eigenvalues ω, $\mathbf{L}(\omega)$ is not invertible. The set of all eigenvalues of $\mathbf{L}$ is referred to as the spectrum. Properties of and solution strategies for general NLEVPs arising in disciplines outside of thermoacoustics are reviewed in [39] and [40].

In the following $\mathbf{L}(\omega)$ is also considered as a function of the parameter n, hence written as $\mathbf{L}(\omega; n)\,\mathbf{p} = 0$. Since $\mathbf{L}(\omega; n)$ depends continuously on n, see Eq. (22), the eigenvalues are also continuous functions of n, see [41, p. 65 and p. 116]. This property permits a nearest-neighbour continuation of the eigenvalues as functions of n and a definition of the origin of a mode as acoustic or intrinsic, depending on whether the mode trajectory parameterized in n tends to an acoustic or and intrinsic mode when $n \to 0$.

Table 1: Acoustic resonance frequencies of the MICCA combustor below 1700 Hz. The azimuthal mode orders m are given, and it is specified in which cavity the modes are dominant. The plenum-dominant modes are of Helmholtz type (approximately constant in axial direction), while the CC-dominant modes exhibit an axial quarter-wave structure. The ninth mode exhibits a minor radial variation but is still of radial order zero. In addition, the first three azimuthal cut-off frequencies f_m^c in the combustion chamber are given according to the analytic expression in [14, p. 138] for an annular geometry.

Index	f in Hz	m	Dominant in
P1	332.09	0	Plenum
P2	471.35	1	Plenum
P3	730.70	2	Plenum
P4	816.64	0	CC
P5	1018.72	3	Plenum
P6	1028.00	1	CC
P7	1316.86	4	Plenum
P8	1499.78	2	CC
P9	1618.79	5	Plenum
$f^c_{m=1}$	633.60	1	CC
$f^c_{m=2}$	1266.78	2	CC
$f^c_{m=3}$	1899.04	3	CC

5. Results and Discussion

The MICCA combustor exhibits 9 distinct acoustic resonance frequencies below 1700 Hz, see Tab. 1. Since the boundary conditions are ideal (fully reflective) and no damping is included, $\mathbf{L}(\omega)$ is self-adjoint, and all passive modes are purely real-valued.

5.1. The complete spectrum below 1700 Hz

Figure 5 shows the spectrum below 1700 Hz, and Table 2 contains the full list of active modes. The active flame effect ($n > 0$) induces a shift in frequency and causes amplification/attenuation of the passive modes. Consequently, the eigenvalues depart from the real axis and enter the complex plane as active modes. This behavior is tracked by gradually increasing $n \in [0, 0.9]$ with a nearest-neighbour

(NN) continuation and shows which modes are of acoustic origin for the final value $n = 0.9$. The stable and unstable half-planes are considered in the range $\mathrm{Im}\,(\omega/2\pi) = \pm 240\,\mathrm{s}^{-1}$. No modes immediately outside this range of growth/attenuation rates were observed. The numerical methods and employed parameters are detailed in AppendixA.

In total, 34 distinct modes (not counting multiplicity) are computed – a significantly higher mode density than previously reported in similar studies. Via NN-continuation, modes of acoustic origin are identified. In addition, a complementary set of intrinsic modes is observed. Azimuthal mode orders are counted from $m = 0$ to $m = 8$ in order to group the intrinsic modes into three clusters. As an additional criterion for grouping the modes, the interaction index n is decreased towards zero, and it is determined whether all modes originate from the same region in the stable half-plane (not depicted here); for details, see Fig. 6. The latter criterion also serves as a test to exclude the possibility that a mode originates from an acoustic resonance frequency outside the considered frequency window.

At the chosen operating conditions, experiments by Durox et al. [42] show that the MICCA combustor exhibits an unstable spinning mode at 457 Hz. The FEM result is consistent with this by predicting an unstable azimuthal mode at 449 Hz, see Fig. 5. For different operating conditions a superposition of two unstable modes was observed by Bourgouin et al. [43] in the form of a slanted mode. The slanted mode originates from an interaction between the unstable azimuthal mode and the neighboring unstable axial mode [44]. The computation predicts additional unstable acoustic modes at higher frequencies, with slightly larger growth rates. These growth rates are likely overestimated since the model does not account for damping effects, which typically increase with frequencies. A further potential source of discrepancy is the fitting of the original FDF of [28] to an n–τ model. Unstable intrinsic modes are predicted but these have comparatively low growth rates. The experimentally observed instability reported in [42] is, thus, due to the acoustic feedback mechanism.

The three clusters are separated by a real spacing of $\Delta f = 1/\tau$ (within almost 1 Hz for the modes of highest azimuthal order). This is precisely the real spacing predicted in Eq. (3), which is also observed in the model problem of Section 3. The surprisingly ordered pattern initially sparked the investigation into the origin of these modes. Modes of the first cluster line up in an orderly fashion. For the second cluster, this is only the case for the upper half of the modes, and for the third cluster, only the two modes of highest azimuthal order do so. If a mode is offset from its cluster, it also no longer adheres to the spacing of $\Delta f = 1/\tau$ and consequently to the 1D result of Eq. (3). Next, it is explained how azimuthal cut-off frequencies affect the offset of intrinsic modes from their respective clusters.

5.2. Azimuthal intrinsic modes of evanescent type

In acoustic waveguides, such as ducts of circular or annular cross section, plane waves, whose amplitude is constant over the duct cross section, always propagate. However, transverse waves propagate along the duct only at frequencies above their respective cut-off frequency; otherwise, these waves experience exponential decay in the axial direction – they are evanescent. The cut-off frequency for a given transverse mode is a function of the cross-sectional geometry and the speed of sound [36]. For the combustion chamber in the MICCA configuration, the cut-off frequencies for the first and second azimuthal mode are given in Tab. 1 and plotted in Figure 5 as dash-dotted lines. Below 1700 Hz, only the two modes of lowest azimuthal mode order are cut-on in the combustion chamber. However, intrinsic modes of much higher mode orders are observed.

The modes of the first cluster depicted in Fig. 5 are all below their respective cut-off frequencies. These modes are confined to the immediate vicinity of the flame, as illustrated on the basis of the modes of azimuthal orders 3 and 8 in Figure 7. A subsequent cut through the modes reveals their evanescent character which increases with mode order, see Fig. 8a.

The axial decay of an evanescent wave in the CC starts just downstream of the flame zone (l_F). Based on Eq. (18) and with the eigenvalues ω from Tab. 2, the axial amplitude distribution of an evanescent wave downstream of the flame takes the form

$$\hat{p}\,(z) \sim e^{-\mathrm{i}k(z-l_\mathrm{F})}\,, \tag{24}$$

where k is given by Eq. (18). Figure 8b shows that the modes of high azimuthal order agree well with the evanescent result of Eq. (24). At a given clustering frequency, the higher the azimuthal order of a mode, the further away it is from its associated

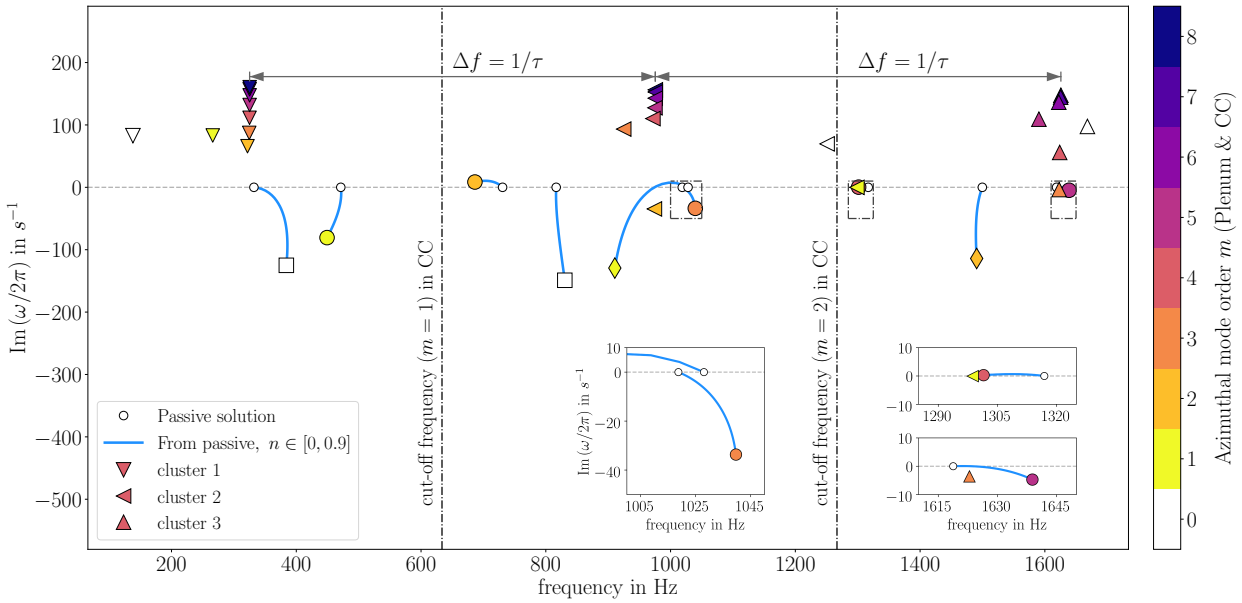

Figure 5: Intrinsic and acoustic modes in the spectrum of the MICCA combustor below 1700 Hz. There are three types of acoustic modes: axial (white squares), azimuthal plenum-dominant (circles) and azimuthal CC-dominant (diamonds). Three clusters of intrinsic CC-dominant modes are observed: 1, 2 and 3 ($\triangledown$, $\triangleleft$ and $\triangle$). The color of the modes corresponds to the respective azimuthal mode order, starting with $m = 0$ (white, axial mode) then $m = 1$ (yellow) and up to $m = 8$ (darkest purple). The dash-dotted boxes mark the windows in the complex plane which are shown enlarged as insets. The paths of the intrinsic modes as functions of n are not depicted here but in Fig. 6.

Table 2: List of active modes depicted in Figure 5, sorted by increasing oscillation frequency. Only azimuthal mode orders m are listed. Except for the $m = 8$ modes, all azimuthal modes ($m > 0$) are degenerate, with multiplicity two. Plenum modes are labeled with (PL) and all other modes are dominant in the CC. The two azimuthal CC modes of acoustic origin are highlighted with a gray background. Intrinsic modes belong to one of the three clusters (symbols $\triangledown, \triangleleft$ and $\triangle$ in Fig. 5.). The azimuthal modes $m = 1, 2$ of cluster 3 are not in the considered frequency range. Between modes #9 and #21 (mode #21 and #32) a real spacing of $\Delta f = 650.37$ Hz (650.12 Hz) is observed, which is approximately $1/\tau = 649.35$ Hz.

No.	f in Hz	Im $\left(\frac{\omega}{2\pi}\right)$ in s^{-1}	m	cluster
1	138.15	+82.79	0	1
2	266.07	+83.11	1	1
3	321.80	+65.91	2	1
4	324.62	+87.27	3	1
5	325.08	+111.46	4	1
6	325.19	+131.94	5	1
7	325.21	+157.21	7	1
8	325.21	+147.46	6	1
9	325.21	+160.55	8	1
10	384.05	−125.01	0 (PL)	acoustic
11	449.32	−80.62	1 (PL)	acoustic
12	686.37	+8.49	2 (PL)	acoustic
13	830.47	−148.97	0	acoustic
14	910.64	−129.42	1	acoustic
15	924.93	+93.36	3	2
16	971.71	+110.15	4	2
17	974.11	−34.66	2	2
18	974.97	+127.47	5	2
19	975.47	+142.86	6	2
20	975.57	+152.81	7	2
21	975.58	+156.23	8	2
22	1039.63	−33.67	3 (PL)	acoustic
23	1250.93	+69.63	0	2
24	1298.73	−0.04	1	2
25	1301.47	+0.29	4 (PL)	acoustic
26	1490.70	−114.07	2	acoustic
27	1590.47	+109.23	5	3
28	1622.36	+136.42	6	3
29	1622.91	−3.59	3	3
30	1623.78	+55.92	4	3
31	1625.35	+144.46	7	3
32	1625.70	+147.69	8	3
33	1638.85	−4.72	5 (PL)	acoustic
34	1668.24	+97.61	0	3

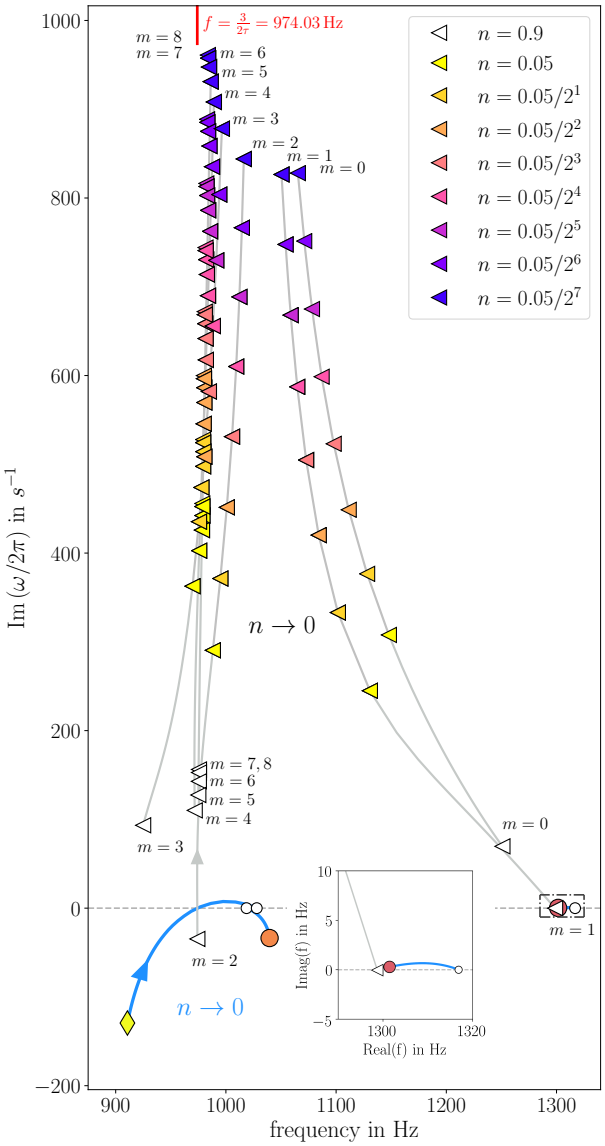

Figure 6: Intrinsic modes of cluster 2 are tracked by decreasing n from 0.9 towards zero. Intrinsic modes are colored by their value of the interaction index n, while acoustic modes are colored by their azimuthal mode order as in Fig. 5. The solid gray lines represent the eigenvalue loci as functions of n. The dash-dotted box marks the window which is shown in the enlarged inset. The modes move to $\mathrm{Im}\,f \to +\infty$ for $n \to 0$. For decreasing n, the eigenvalues corresponding to different azimuthal mode orders move closer; in fact, as n tends to zero, all eigenvalues in a cluster merge. This is explained in Section 5.3. For comparison the frequency for $j = 1$ in Tab. 3 is included as a small vertical red line. Cut-on intrinsic modes exhibit complex paths, e.g., $m = 0, 1$ of cluster 2 span a wide range of oscillation frequencies as a function of n, while cut-off intrinsic modes only move to higher damping rates. The acoustic (yellow diamond) and intrinsic (left pointing white triangle labelled with $m = 2$) modes do not intersect for a certain n. Both modes pass the same point but for a different n.

Table 3: Frequencies according to Eq. (1) for a 1D Rijke tube with anechoic terminations and the frequencies of the intrinsic modes in the MICCA combustor with the strongest evanescent character (highest azimuthal mode order in their respective cluster) from Tab. 2.

	$j = 0$	$j = 1$	$j = 2$
$\frac{\pi(2j+1)}{\tau}$	324.68 Hz	974.03 Hz	1623.38 Hz
	cluster 1	cluster 2	cluster 3
$m = 8$	325.21 Hz	975.58 Hz	1625.70 Hz

cut-off frequency and the stronger is the axial attenuation. This is visible in the mode shape as a strong exponential decay in longitudinal direction. If the longitudinal decay is sufficiently strong, the mode is unaffected by the outlet boundary condition, see the modes of high azimuthal order in Fig. 8b. This is an environment somewhat similar to anechoic boundary conditions that were shown to facilitate 'pure' intrinsic modes [16, 45, 18, 19].

Table 3 lists the observed frequencies and the values predicted by Eq. (1). A strong similarity is evident, even though the cut-off modes experience very different boundary conditions. The stronger cut-off a mode is, the closer its frequency is to the one-dimensional result for anechoic terminations of Eq. (1). The difference in boundary conditions does not appear to affect the frequencies. However, amplification/attenuation rates do not agree: Eq. (1) gives $\mathrm{Im}\,(\omega/2\pi) = +10.89\,\mathrm{s}^{-1}$ while all clustered intrinsic modes in the MICCA combustor are damped much stronger.

Figure 5 shows that the mode of azimuthal order $m = 1$ is visibly offset from the first cluster of intrinsic modes. In the second cluster, modes $m = 1, 2, 3$ are offset and mode $m = 2$ is even cut-on. The relation between the degree of the cut-off and offset from a cluster can be explained by considering the cut through the mode shapes in Figure 9. Modes $m = 2, 3$ are cut-off but the exponential decay is not strong enough: the modes still have to fulfill the outlet boundary condition. Modes of higher order than $m = 3$ have essentially decayed to zero before the outlet. Even though a mode is cut-off, if its mode shape is affected by the boundary condition, then so is its frequency. A shift in the frequency away from the cluster then occurs, and the eigenvalue expression from the one-dimensional case, Eq. (1), does no longer hold. The modes experience acoustic reflection at the outlet and are, thus, not purely intrinsic anymore. Most clearly, the cut-on mode $m = 1$ of cluster 2 shows a dis-

tinct quarter-wave structure, very different from the evanescent modes of higher azimuthal order in its cluster. For the third cluster, more modes exhibit this behavior, since even more modes are close, or even above, their respective cut-off frequencies.

The spectrum also contains three intrinsic modes of axial type. These are always cut-on and, hence, offset from their respective cluster.

The pattern in Fig. 6 for $n = 0.05$ is qualitatively similar to the pattern observed in the results from the analytical model (Fig. 2). In the latter case, less offset of individual modes from their respective cluster is observed and grouping is straightforward.

5.3. The limiting case of an acoustically weak flame

As discussed in Section 1.1 on the basis of Eq. (1), the frequency spacing between two intrinsic modes in a Rijke tube with anechoic boundaries is $\Delta f = 1/\tau$. One can furthermore deduce from Eq. (1) that $\mathrm{Im}\,\omega \to +\infty$, as $n \to 0$. Figure 6 shows that all modes of non-acoustic origin exhibit increasingly higher damping rates as the interaction index tends to zero, consistent with the theoretical prediction. Consequently, every mode not originating from a passive acoustic mode is considered of intrinsic origin. Figure 6 also shows that intrinsic modes close to or above their respective cut-off frequency ($m = 0, 1, 2$ in the figure) exhibit non-trivial trajectories as functions of n. Cut-off intrinsic modes remain close to one frequency for all values of n and only show a change in their imaginary part.

In each intrinsic cluster, only modes up to azimuthal order $m = 8$ are observed. In contrast, in the analytical model, modes of arbitrarily high azimuthal order can be found.

Modes of acoustic origin (or purely acoustic modes in systems without flame response) in an annular combustor can have much higher azimuthal orders than half the number of burners; in fact, the azimuthal order can be arbitrarily high. Bloch-wave theory ascertains that all modes can be represented with Bloch wave numbers up to ± 8. But the equivalence between Bloch wave number and azimuthal mode order holds only for small azimuthal mode orders (see Mensah et al. [12]). Modes of any azimuthal order can still be represented with Bloch wave numbers up to ± 8 because waves can form on the sub-unit-cell scale. For example, a mode of azimuthal order 9 can be represented as a Bloch wave with Bloch wave number 7; the part of the solution that is periodic on the unit cell then hosts one wave length on the cell.

The maximally observed mode order is explained by considering the limit $n \to 0$ for the intrinsic modes in one cluster. As we know from previous studies on intrinsic modes, and as also our results in the present work show, the growth rates of intrinsic modes tend to negative infinity as $n \to 0$, see Fig. 6. In this limit, the modes are infinitely confined to the immediate vicinity of the flame, as they are infinitely damped ($\mathrm{Im}\,\omega \to \infty$). But then the flames do not affect each other and become effectively uncoupled. This situation is conceptually similar to 16 identical but isolated combustors. Such a configuration must exhibit a 16-fold degeneracy because each combustor has the same eigenvalues (as they are identical and uncoupled). This degeneracy is semi-simple, i.e. it has a full eigenspace with finite eigenvalue sensitivity. It is easy to see that these eigenvalues are not defective; in fact, an obvious basis for the degenerate eigenspace is the set of the 16 individual flame modes. An alternative basis is given by a set of 16 Bloch waves that recombine the 16 individual flame modes by modulating them according to the 16 sixteen-point discrete Fourier modes. It is the latter basis into which the degenerate eigenspace unfolds when n is perturbed from zero. As soon as $n > 0$, the intrinsic modes exhibit only finite damping ($\mathrm{Im}\,\omega < \infty$) and the flames start communicating so that the system becomes fully coupled. The only degeneracy that remains is that generally associated with 16-fold discrete rotational symmetry, i.e. modes of azimuthal order 0 and multiples of 8 being simple and all others being two-fold degenerate. However, the sum of all algebraic multiplicities of all eigenvalues in one cluster must be conserved (i.e. it remains 16 for all values of n) because the eigenvalues are continuous functions of the parameter (here, the interaction index n), see [41, p. 65 and p. 116]. Assuming that the lower-order azimuthal modes are populated first, the total algebraic multiplicity of 16, originating from the $n \to 0$ limit, is only sufficient to go up to azimuthal order $m = 8$ (because modes with $m = 1 \ldots 7$ are two-fold degenerate).

5.4. Proximity of intrinsic modes to acoustic modes

Figure 5 shows that intrinsic modes are located in close proximity to modes of acoustic origin. The two right insets in Fig. 5 depict the two cases with the modes being closest. Evidently, modes of intrinsic origin can appear not only at non-acoustic resonance frequencies, but also very close to the passive acoustic modes. As a consequence, the nature of a

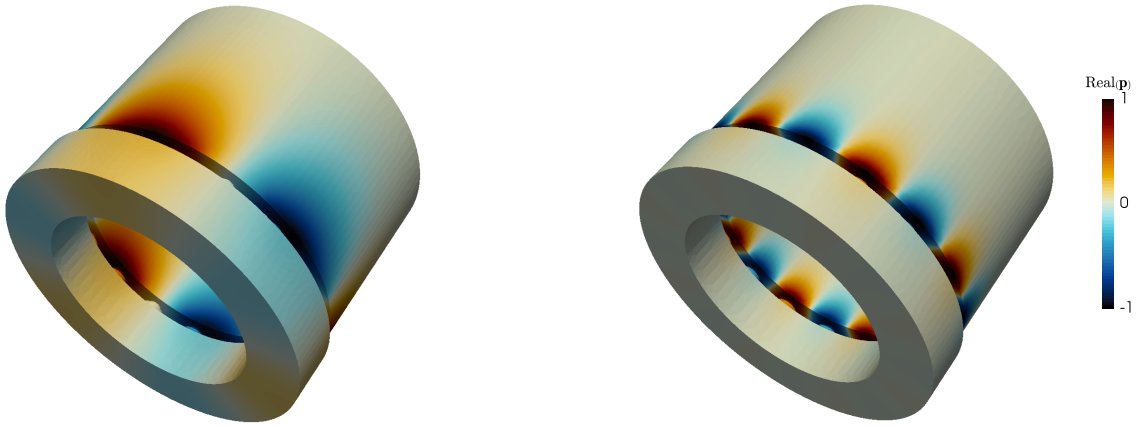

(a) Mode #4 ($\bigtriangledown, m = 3$)

(b) Mode #9 ($\bigtriangledown, m = 8$)

Figure 7: Real part of the azimuthal modes $m = 3, 8$ of cluster 1, see Fig. 5 and Tab. 2. Mode #4 is degenerate, but only one mode in the degenerate pair is depicted. The modes are dominant at the inlet to the combustion chamber. Mode #4, with lower azimuthal order, extends further into the CC than #9, which is of higher mode azimuthal order. This trend is confirmed for the remaining modes of cluster 1 ($m = 2, 4, 5, 6, 7$).

mode cannot be established by its frequency only but requires analysis of the mode shape or its locus in the complex plane as a function of the interaction index n (or another suitable parameter).

5.5. Unstable intrinsic modes

Three intrinsic modes are unstable for $n = 0.9$, see Table 2. Figure 10 contains the values of n for which all intrinsic modes depicted in Fig. 5 become unstable. NN-continuation is conducted to obtain the unstable n values, but the computation is not continued for modes that remain stable for $n < 10$. The majority of modes of intrinsic origin become unstable for sufficiently high n. In addition, it can be observed that modes of higher frequencies, closer to or below their respective cut-off frequencies, become unstable for lower values of the interaction index than modes of lower frequencies.

Two unstable intrinsic modes of special interest can be seen in Figure 6 for $n = 0.9$. Both modes originate from the same cluster. One mode ($m = 1$) is cut-on and marginally unstable, while the other ($m = 2$) is unstable in spite of being cut-off. Somewhat unexpectedly, the mode of higher azimuthal mode order is encountered at a lower frequency and exhibits a larger growth rate.

6. Conclusion

The intrinsic feedback mechanism in annular thermoacoustic systems is illustrated on the basis of an annular laboratory model combustor. Modes originating from the intrinsic mechanism form clusters, with frequencies that correspond to those of intrinsic modes in a simple single-flame Rijke tube.

The clustering of the eigenvalues is related to the acoustic cut-off mechanism for non-planar modes. In fact, it is demonstrated that the evanescent character of cut-off azimuthal modes provides an environment similar to non-reflective boundary conditions, hence the concurrence with intrinsic modes in an anechoic single-flame setup. This environment allows intrinsic modes of different azimuthal orders to exist at very close frequencies and, thus, to form clusters. However, not all intrinsic modes are clustered. Those that are too close or even above their cut-off frequency are affected by the outlet boundary condition. This is visible as a marked offset from the intrinsic eigenvalue cluster.

The intrinsic mechanism scrutinized in this work is not new per se. It is of the same origin as in single-flame systems, where it has been studied in detail over the last 5 years. In the present work, it was shown how the very same mechanism manifests itself in an annular geometry in the form of intrinsic azimuthal modes, and the crucial role of the cut-off mechanism was highlighted. In the present configuration, the modes with the largest growth rates are not intrinsic and would not be observed in experiments. An increase of acoustic losses at the boundaries could dampen the acoustic modes to a point at which an intrinsic mode is the most

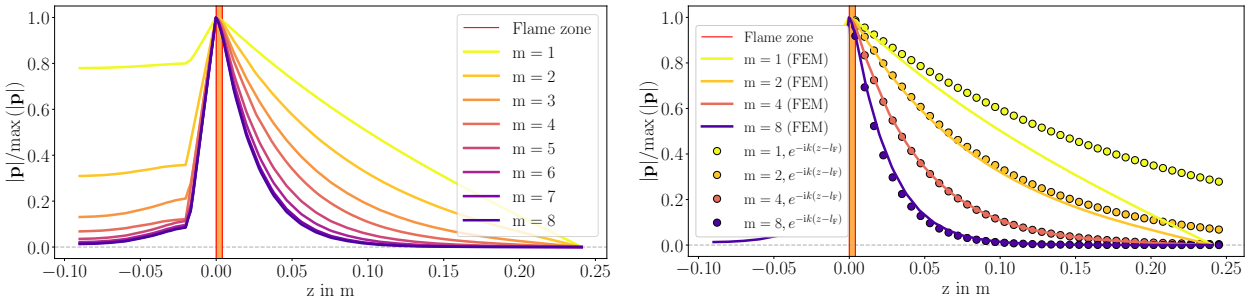

(a) (b)

Figure 8: Cluster 1: normalized absolute value of the pressure $\mathbf{p}$ over the axial coordinate along a burner axis for azimuthal modes.. The colors correspond to the colors in Fig. 5. Left: All modes are cut-off and a higher mode order corresponds to a stronger cut-off. The mode with $m = 1$ is just barely cut-off. Right: FEM result (solid line) and ansatz for evanescent waves Eq. (24) (dots). The ansatz matches well for strongly cut-off modes. Modes of low azimuthal mode numbers are weakly cut-off and experience the pressure node boundary condition at the outlet: the mode shapes deviate from the purely evanescent character as Eq. (24) does not account for reflective boundary conditions.

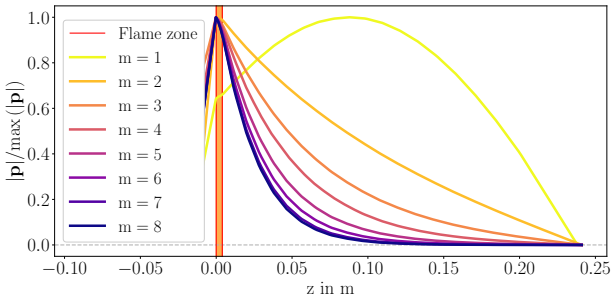

Figure 9: Cluster 2: normalized absolute value of the pressure $\mathbf{p}$ over the axial coordinate along a burner axis for intrinsic modes of different azimuthal orders. Mode $m = 1$ is cut-on and exhibits a distinct quarter-wave shape. Modes $m = 2, 3$ are cut-off but the exponential decay is not sufficiently strong so that they are affected by the pressure node at the outlet. Both modes deviate from the purely evanescent character and are consequently offset from their cluster, see the spectrum in Fig. 5 and for more detail Fig. 6.

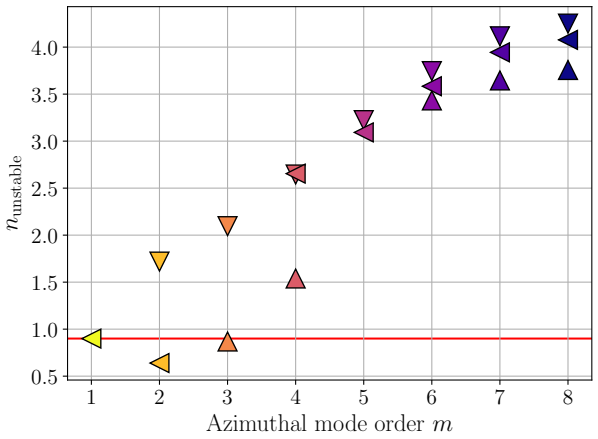

Figure 10: The values of the interaction index, for which the intrinsic modes enter the unstable half-plane. Markers and colors chosen according to Fig. 5. The red line corresponds to the value $n = 0.9$. Modes #1 ($\triangledown, m = 1$), #14 ($\triangleleft, m = 3$) and #26 ($\triangle, m = 5$) did not become unstable for $n < 10$ and are, thus, not depicted. For these modes the computation was not continued further. Note that the modes of cluster 3 with $m = 1, 2$ are outside of the considered frequency range and not investigated here. The axial intrinsic modes (not depicted here) become unstable for $n = 2.613$ (mode #23), $n = 3.140$ (mode #34) and mode #1 did not become unstable for $n < 10$.

unstable one; this would potentially facilitate observing a thermoacoustic mode of intrinsic origin experimentally.

For the first time, a systematic and complete description of the thermoacoustic spectrum of an annular combustor was given. Previously, this has only been available for single-flame configurations. The intrinsic mechanism explored in this paper can be expected to be generically present in all annular acoustic configurations with flame response. We conjecture that earlier numerical studies of thermoacoustic modes in annular combustion chambers did not observe intrinsic mode clusters because they are challenging to find numerically with iterative methods. In the present work, the non-iterative method of Beyn [32] was utilized for the solution of the nonlinear eigenvalue problem associated with the thermoacoustic Helmholtz equation. This was essential in determining all eigenvalues of acoustic and intrinsic origin.

References

[1] T. Poinsot, Prediction and control of combustion instabilities in real engines, Proc. Combust. Inst. 36 (1) (2017) 1–28.

[2] T. C. Lieuwen, V. Yang (Eds.), Combustion Instabilities in Gas Turbine Engines, Vol. 210 of Prog. Astronaut. Aeronaut., AIAA, Inc., 2005.

[3] G. Staffelbach, L. Gicquel, T. Poinsot, Large eddy simulation of self-excited azimuthal modes in annular combustors, Proc. Combust. Inst. 32 (2) (2009) 2909–2916.

[4] P. Wolf, G. Staffelbach, L. Gicquel, D. Müller, T. Poinsot, Acoustic and large eddy simulation studies of azimuthal modes in annular combustion chambers, Combust. Flame 159 (2012) 3398–3413.

[5] J. Gikadi, Prediction of acoustic modes in combustors using linearized Navier-Stokes equations in frequency space, Ph.D. thesis, Technische Universität München (2014).

[6] M. Schulze, T. Hummel, N. Klarmann, F. Berger, B. Schuermans, T. Sattelmayer, Linearized Euler equations for the prediction of linear high-frequency stability in gas turbine combustors, J. Eng. Gas Turbines Power 139 (3) (2017) 031510 (10 pages).

[7] F. Nicoud, L. Benoit, C. Sensiau, T. Poinsot, Acoustic modes in combustors with complex impedances and multidimensional active flames, AIAA J. 45 (2) (2007) 426–441.

[8] S. Evesque, W. Polifke, Low-order acoustic modelling for annular combustors: Validation and inclusion of modal coupling, ASME paper GT-2002-30064, 2002.

[9] B. Schuermans, V. Bellucci, C. O. Paschereit, Thermoacoustic modeling and control of multi burner combustion systems, ASME paper 2003-GT-38688, 2003.

[10] T. Sattelmayer, W. Polifke, Assessment of methods for the computation of the linear stability of combustors, Combust. Sci. Technol. 175 (2003) 453–476.

[11] S. M. Camporeale, B. Fortunator, G. Campa, A finite element method for three-dimensional analysis of thermo-acoustic combustion instability, J. Eng. Gas Turbines Power 133 (2011) 015506 (13 pages).

[12] G. A. Mensah, G. Campa, J. P. Moeck, Efficient computation of thermoacoustic modes in industrial annular combustion chambers based on Bloch wave theory, J. Eng. Gas Turbines Power 138 (2016) 081502 (7 pages).

[13] M. Bauerheim, F. Nicoud, T. Poinsot, Progress in analytical methods to predict and control azimuthal combustion instability modes in annular chambers, Phys. Fluids 28 (2016) 021303 (27 pages).

[14] T. C. Lieuwen, Unsteady Combustor Physics, Cambridge University Press, 2012.

[15] P. Hoeijmakers, Flame-acoustic coupling in combustion instabilities, Ph.D. thesis, Technische Universiteit Eindhoven (2014).

[16] M. Hoeijmakers, V. Kornilov, I. L. Arteaga, P. de Goey, H. Nijmeijer, Intrinsic instability of flame–acoustic coupling, Combust. Flame 161 (11) (2014) 2860–2867.

[17] S. Bomberg, T. Emmert, W. Polifke, Thermal versus acoustic response of velocity sensitive premixed flames, Proc. Combust. Inst. 35 (3) (2015) 3185–3192.

[18] T. Emmert, S. Bomberg, W. Polifke, Intrinsic thermoacoustic instability of premixed flames, Combust. Flame 162 (1) (2015) 75–85.

[19] N. K. Mukherjee, V. Shrira, Intrinsic flame instabilities in combustors: Analytic description of a 1-d resonator model, Combust. Flame 185 (2017) 188–209.

[20] E. Courtine, L. Selle, T. Poinsot, DNS of intrinsic thermoacoustic modes in laminar premixed flames, Combust. Flame 162 (11) (2015) 4331–4341.

[21] K. R. McManus, T. Poinsot, S. Candel, A review of active control of combustion instabilities, Prog. Energy Combust. Sci. 19 (1) (1993) 1–29.

[22] A. Orchini, C. F. Silva, G. A. Mensah, J. P. Moeck, Thermoacoustic modes of intrinsic and acoustic origin and their interplay with exceptional points, accepted for publication in Combust. Flame.

[23] P. E. Buschmann, G. A. Mensah, F. Nicoud, J. P. Moeck, Solution of thermoacoustic eigenvalue problems with a non-iterative method, ASME paper GT2019-90834, 2019.

[24] E. Courtine, L. Selle, F. Nicoud, W. Polifke, C. Silva, M. Bauerheim, T. Poinsot, Causality and intrinsic thermoacoustic instability modes, in: Proceedings of the summer program, Center for Turbulence Research, 2014, p. 169.

[25] C. F. Silva, M. Merk, T. Komarek, W. Polifke, The contribution of intrinsic thermoacoustic feedback to combustion noise and resonances of a confined turbulent premixed flame, Combustion and Flame 182 (2017) 269–278.

[26] A. Ghani, T. Steinbacher, A. Albayrak, W. Polifke, Intrinsic thermoacoustic feedback loop in turbulent spray flames, Combust. Flame 205 (2019) 22–32.

[27] J.-F. Bourgouin, D. Durox, J. Moeck, T. Schuller, S. Candel, Self-sustained instabilities in an annular combustor coupled by azimuthal and longitudinal acoustic modes, ASME paper GT2013-95010, 2013.

[28] J.-F. Bourgouin, D. Durox, J. Moeck, T. Schuller, S. Candel, Characterization and modeling of a spinning thermoacoustic instability in an annular combustor equipped with multiple matrix injectors, J. Eng. Gas Turbines Power 137 (2) (2015) 021503 (11 pages).

[29] D. Laera, K. Prieur, D. Durox, T. Schuller, S. Camporeale, S. Candel, Flame describing function analysis of standing modes in an annular combustor and comparison with experiments, in: Thermoacoustic Instabilities in Gas Turbines and Rocket Engines: Industry meets Academia, Paper No: GTRE-044, Munich, Germany, 2016.
[30] D. Laera, K. Prieur, D. Durox, T. Schuller, S. Camporeale, S. Candel, Impact of heat release distribution on the spinning modes of an annular combustor with multiple matrix burners, J. Eng. Gas Turbines Power 139 (5) (2017) 051505 (10 pages).
[31] D. Laera, G. Campa, S. Camporeale, A finite element method for a weakly nonlinear dynamic analysis and bifurcation tracking of thermo-acoustic instability in longitudinal and annular combustors, Applied energy 187 (2017) 216–227.
[32] W.-J. Beyn, An integral method for solving nonlinear eigenvalue problems, Linear Algebra Appl. 436 (2012) 3839–3863.
[33] L. Crocco, S.-I. Cheng, Theory of combustion instability in liquid propellant rocket motors, AGARDograph No. 8, Butterworths Scientific Publications, 1956.
[34] W. Polifke, C. O. Paschereit, K. Döbbeling, Constructive and destructive interference of acoustic and entropy waves in a premixed combustor with a choked exit, Int. J. Acoust. Vibr. 6 (3) (2001) 135–146.
[35] D. Yang, A. S. Morgans, Low-order network modeling for annular combustors exhibiting longitudinal and circumferential modes, in: ASME Turbo Expo 2018: Turbomachinery Technical Conference and Exposition, American Society of Mechanical Engineers, 2018, pp. V04BT04A026–V04BT04A026.
[36] S. W. Rienstra, A. Hirschberg, An introduction to acoustics, Eindhoven University of Technology, 2018.
[37] C. F. Silva, K. J. Yong, L. Magri, Thermoacoustic modes of quasi-one-dimensional combustors in the region of marginal stability, J. Eng. Gas Turbines Power 141 (2) (2019) 021022.
[38] G. A. Mensah, P. E. Buschmann, A. Orchini, J. P. Moeck, Pyholtz, https://bitbucket.org/pyholtzdevelopers/public.git (2018).
[39] S. Güttel, F. Tisseur, The nonlinear eigenvalue problem, Acta Numer. 26 (2017) 1–94.
[40] V. Mehrmann, H. Voss, Nonlinear eigenvalue problems: a challenge for modern eigenvalue methods, GAMM-Mitteilungen 27 (2) (2014) 121–152.
[41] T. Kato, Perturbation theory for linear operators, 2nd Edition, Springer Berlin/Heidelberg, New York, 1980.
[42] D. Durox, J.-F. Bourgouin, J. P. Moeck, M. Philip, T. Schuller, S. Candel, Nonlinear interactions in combustion instabilities coupled by azimuthal acoustic modes, in: Proceedings of the International Summer School and Workshop on Non-Normal and Nonlinear Effects in Aero- and Thermoacoustics, Munich, 2013.
[43] J.-F. Bourgouin, D. Durox, J. Moeck, T. Schuller, S. Candel, A new pattern of instability observed in an annular combustor: the slanted mode, Proc. Combust. Inst. 35 (2015) 3237–3244.
[44] J. P. Moeck, D. Durox, T. Schuller, S. Candel, Nonlinear thermoacoustic mode synchronization in annular combustors, Proc. Combust. Inst. 37 (2019) 5343–5350.
[45] C. F. Silva, T. Emmert, S. Jaensch, W. Polifke, Numerical study on intrinsic thermoacoustic instability of a laminar premixed flame, Combust. Flame 162 (2015) 3370–3378.
[46] G. A. Mensah, L. Magri, C. F. Silva, P. E. Buschmann, J. P. Moeck, Exceptional points in the thermoacoustic spectrum, J. Sound Vib. 433 (2018) 124–128.
[47] P. Lancaster, A generalised Rayleigh quotient iteration for lambda-matrices, Archive for Rational Mechanics and Analysis 8 (1) (1961) 309.

Table A.4: Parameters employed in Beyn's method (see [32] and [23] for details) and Newton iterations. Beyn's method is performed with a series of overlapping circles of radius 160 Hz to obtain the results in Figure 5. All eigenvalues presented in this paper have been converged in the Newton method using the listed parameters, with the values obtained by Beyn's method as initial guesses.

l	N	tol_{σ}
32	72	1.0×10^{-10}
$\mathrm{tol}_{\Delta\omega}$	$\mathrm{tol}_{\mathrm{residual}}$	relaxation
1.0×10^{-4}	1.0×10^{-4}	0.5

AppendixA. Numerical solution of the nonlinear eigenvalue problem

The problem size of $\mathbf{L}(\omega)$ in Eq. (23) prohibits the use of root-finding algorithms to the determinant $\det \mathbf{L}(\omega)$. Two applicable solution strategies are briefly described in this appendix: a non-iterative strategy based on contour integration due to Beyn [32] and a Newton-based iterative algorithm.

Both methods are part of the NLEVP-solution routines of PyHoltz [38]. The parameters employed in both methods to obtain the results of Section 5.1 are listed in Tab. A.4.

AppendixA.1. Beyn's method based on contour integration

The original work of Beyn [32] extensively covers the technical details of his method. A concise and less technical description of the theoretical background and guidelines for the application to thermoacoustic problems are given in [23]. We refer to both papers for details and only summarize the main ideas of the technique here. Beyn's method returns all eigenvalues and corresponding eigenvectors in a user-specified contour in the complex plane.

In short, two variants of the inverse $\mathbf{L}(z)^{-1}$ of Eq. (23) are numerically integrated along a closed contour Γ in the complex plane, specified by the

user:

$$\oint_\Gamma z^p \mathbf{L}(z)^{-1} \hat{\mathbf{V}} \, \mathrm{d}z \approx \sum_{j=0}^{N-1} \alpha_j z_j^p \mathbf{L}(z_j)^{-1} \hat{\mathbf{V}} \quad (A.1)$$
$$= \mathbf{A}_p \ , \ p \in \{0, 1\} \ .$$

Gauss–Legendre integration with N sampling points z_j and corresponding weights α_j is used for computing the moment matrices $\mathbf{A}_0$ and $\mathbf{A}_1$. The contour Γ is the window of interest, spanning the oscillation frequencies and amplification/attenuation rates to be considered. The algorithm avoids complete inversion of $\mathbf{L}(z_j)$ to reduce numerical cost by solving the linear equation system $\mathbf{L}(z_j)^{-1} \hat{\mathbf{V}}$ at every sampling point. The random matrix $\hat{\mathbf{V}} \in \mathbb{C}^{d \times l}$ is chosen s.t. the number of columns l is smaller than the expected sum of the geometric multiplicities of all eigenvalues inside Γ. The parameter l needs to be chosen with care to limit computational cost. A discussion of an adequate choice for thermoacoustic applications can be found in [23]. From the $\mathbf{A}_p$ matrices all eigenpairs inside the contour Γ are obtained following an advantageous decomposition, see [32].

Simple, semi-simple and even defective eigenvalues can be computed. This technique is, thus, suitable for systems with spatial symmetries and for the recently discussed exceptional points [46]. Beyn's method can be employed as a black box solver for arbitrary NLEVPs but requires $\mathbf{L}(\omega)$ to depend analytically on ω, which is fulfilled in the present formulation due to the n–τ model and the chosen boundary conditions.

AppendixA.2. Iterative method

In Beyn's method the matrices $\mathbf{A}_p$ have to be computed with an increase in the number of sampling points N (or l) to establish convergence, which is a costly step. Instead it is less costly and quicker to perform Beyn's method once and enter the result into a locally convergent iterative method. A Newton method that is known as generalized Rayleigh quotient iteration [47] is employed for this purpose. The method reformulates the problem as a linear eigenvalue problem

$$\mathbf{L}(\omega)\mathbf{p} = \lambda \mathbf{M}\mathbf{p} \quad (A.2)$$

in the auxiliary eigenvalue λ. Finding ω such that $\lambda = 0$ solves the original eigenvalue problem Eq. (22). First order perturbation theory is used to compute the derivative $\frac{\mathrm{d}\lambda}{\mathrm{d}\omega}$ and, thus, facilitates a Newton iteration to solve the problem. With good initial values the Newton method converges in a hand-full of iterations.

To establish convergence, two criteria are checked: a tolerance on the residual following [32] (with $\mathbf{p}$ normalized in $||\cdot||_2$), and the relative change in the eigenvalue:

$$||\mathbf{L}(\omega)\,\mathbf{p}||_2 < \mathrm{tol}_{\mathrm{residual}} \ , \quad (A.3)$$

$$\frac{|\omega_{i+1} - \omega_i|}{|\omega_i|} < \mathrm{tol}_{\Delta\omega} \ . \quad (A.4)$$

Iterative algorithms require good initial values. The acoustic resonance frequencies are a suitable choice to compute the modes of acoustic origin. The results in this paper demonstrate that the intrinsic modes can appear seemingly anywhere in the complex plane. Therefore, a suitable initial value is hard to come up with for intrinsic modes. Here, Beyn's method is the ideal tool to compute these. As a double check, eigenvalues from Beyn's method are entered into the Newton method, because Beyn's method can return numerically spurious eigenvalues, see [23] for details and a discussion.